scientific reports

Check for updates

OPEN

Differentiation between non-small cell lung cancer and radiation pneumonitis after carbon-ion radiotherapy by ^{18}F-FDG PET/CT texture analysis

Makito Suga[1,2,3], Ryuichi Nishii[1✉], Kenta Miwa[4], Yuto Kamitaka[3], Kana Yamazaki[1], Kentaro Tamura[1], Naoyoshi Yamamoto[3], Ryosuke Kohno[3], Masato Kobayashi[5], Katsuyuki Tanimoto[3], Hiroshi Tsuji[3] & Tatsuya Higashi[1]

The differentiation of non-small cell lung cancer (NSCLC) and radiation pneumonitis (RP) is critically essential for selecting optimal clinical therapeutic strategies to manage post carbon-ion radiotherapy (CIRT) in patients with NSCLC. The aim of this study was to assess the ability of ^{18}F-FDG PET/CT metabolic parameters and its textural image features to differentiate NSCLC from RP after CIRT to develop a differential diagnosis of malignancy and benign lesion. We retrospectively analyzed ^{18}F-FDG PET/CT image data from 32 patients with histopathologically proven NSCLC who were scheduled to undergo CIRT and 31 patients diagnosed with RP after CIRT. The SUV parameters, metabolic tumor volume (MTV), total lesion glycolysis (TLG) as well as fifty-six texture parameters derived from seven matrices were determined using PETSTAT image-analysis software. Data were statistically compared between NSCLC and RP using Wilcoxon rank-sum tests. Diagnostic accuracy was assessed using receiver operating characteristics (ROC) curves. Several texture parameters significantly differed between NSCLC and RP ($p < 0.05$). The parameters that were high in areas under the ROC curves (AUC) were as follows: SUV_{max}, 0.64; GLRLM run percentage, 0.83 and NGTDM coarseness, 0.82. Diagnostic accuracy was improved using GLRLM run percentage or NGTDM coarseness compared with SUV_{max} ($p < 0.01$). The texture parameters of ^{18}F-FDG uptake yielded excellent outcomes for differentiating NSCLC from radiation pneumonitis after CIRT, which outperformed SUV-based evaluation. In particular, GLRLM run percentage and NGTDM coarseness of ^{18}F-FDG PET/CT images would be appropriate parameters that can offer high diagnostic accuracy.

Lung cancer is one of the most prevalent cancers worldwide, with non-small cell lung cancer (NSCLC) accounting for 85% to 90% of all forms of lung cancer[1]. Radiotherapy is an option for patients who are unable to tolerate or who decline surgery. Stereotactic body radiotherapy[2] and particle therapy[3] have been widely applied to such patients. Carbon-ion radiotherapy (CIRT) has excellent dose-localizing properties[4], and can thus deliver a high dose to a target while avoiding adjacent critical organs at risk. The high radiosensitivity of the lungs constitutes a critical dose-limiting factor for treating thoracic tumors with radiation[5,6]. Various pulmonary side effects can arise after CIRT, such as radiographic lung damage, pleural reactions, pneumonitis, or fibrosis[7,8].

Generally, CT cannot distinguish necrotic tumors or fibrotic scar tissues from residual or recurrent tumors[9], which leads to a delay before undergoing repeat CIRT. On the other hand, metabolic imaging using ^{18}F-fluoro-deoxyglucose (^{18}F-FDG) positron emission tomography/computed tomography (^{18}F-FDG PET/CT) can

discriminate between recurrence and post-treatment changes[10–12], since ^{18}F-FDG PET/CT can noninvasively indirectly measure glucose metabolism in vivo.

The maximum standardized uptake value (SUV$_{max}$) is the most prevalent parameter used to estimate tumor metabolic activity in ^{18}F-FDG PET/CT images. However, the SUV$_{max}$ is measured as the most numerous pixels in a region of interest; images show only areas of the highest intensity of ^{18}F-FDG uptake in a tumor and cannot reflect metabolic activity in whole tumors[13]. Therefore, the extent of active lesions in malignant tumors and active residual lesions after treatment is difficult to ascertain using SUV$_{max}$ accurately. To overcome these issues, metabolic tumor volume (MTV) and total lesion glycolysis (TLG) have been proposed as supplementary diagnostic indicators of tumor activity[14].

Few studies have discriminated lung cancer from radiation pneumonitis (RP) in images based on accumulated ^{18}F-FDG. This suggests that ^{18}F-FDG uptake after RT might be due not only to recurrent tumors but also to RT-induced inflammation. The characterization of uptake heterogeneity is gaining popularity through radiomics-based analyses that extract high throughput features based on intensity, shape, and the texture of uptake within regions of interest. Using textural features has improved the ability of ^{18}F-FDG PET/CT to discriminate abnormal from normal tissues and delineate lesions. Textural features derived from Neighboring Gray Tone Difference Matrices describe features such as coarseness, contrast, and busyness on PET images[15]. They can differentiate cancerous tumors of the head and neck from normal tissues[16]. However, whether textural features can discriminate malignant from benign lesions remains unknown. The value of quantitative heterogeneity in ^{18}F-FDG PET/CT images for RP after CIRT has not also been investigated. The aim of this study was to assess the ability of ^{18}F-FDG PET/CT metabolic parameters and its textural image features to differentiate NSCLC from RP after CIRT to develop a differential diagnosis of malignancy and benign lesion.

Methods

Patients.   We retrospectively analyzed ^{18}F-FDG PET/CT data obtained from 32 patients with NSCLC who underwent ^{18}F-FDG PET/CT before CIRT (50.0 GyE/day), and from 31 patients with RP who were diagnosed by biopsy or by clinical follow up at > 1 year after CIRT (50.0 GyE/day) for NSCLC. The NSCLC patients had not received chemotherapy before CIRT and underwent ^{18}F-FDG PET/CT at baseline.

This clinical study was approved by the Ethics Committee at the National Institute of Radiological Sciences (Approval No. 19–019), and written informed consent was obtained from all patients. This study was conducted as a research involving research participants in accordance with the principles outlined in the 1964 Declaration of Helsinki and its later amendments. The results of this retrospective study did not influence further therapeutic decision-making.

^{18}F-FDG PET/CT.   Patients fasted for at least 6 h before being injected with 4 MBq/kg ^{18}F-FDG. Whole-body images were acquired at a mean of 60 min later after voiding from the top of the skull to the midthigh using an Aquiduo PET/CT scanner (Canon Corp., Japan). Aquiduo PET/CT scanner has the following technical characteristics: detector material, Lu$_2$SiO$_5$(Ce) (LSO); crystal size, $4.0 \times 4.0 \times 20$ mm^3; detector ring diameter, 830 mm; transaxial field of view (FOV), 585 mm; axial FOV, 162 mm, coincidence window, 4.5 ns; energy window, 425–650 keV; maximum ring difference, 27; random correction, delayed; scatter correction, single scatter simulation. Emission data were acquired for 2–3 min per bed position[17]. The PET images were reconstructed using an iterative algorithm (the combination of Fourier rebinning and the ordered subsets expectation–maximization [FORE + 2D-OSEM]; 4 iterations, 14 subsets) with an 8-mm Gaussian filter, a 128×128 matrix (3.9 mm/pixel) and 81 slices (2 mm/slice). Time-of-flight and point spread function correction were not applied. The spatial resolution of this scanner according to NEMA NU 2–2007 is 6.5 mm in full width at half maximum (FWHM) at 10 mm off center. Whole-body spiral CT scanning proceeded under the following parameters: 120 kV; auto exposure control (noise level: SD 10); 512×512 matrix; beam pitch, 0.94; 2 mm $\times$ 16-row mode. The CT data were used for the attenuation correction.

Quantitative analysis.   We used the PET/CT medical imaging viewer, PETSTAT (AdIn Research Inc., Tokyo, Japan) for texture analysis. Volumes of interest (VOI) on tumors were delineated using a threshold of 40% (40P) of the SUV$_{max}$ in each lesion. In the texture analysis of ^{18}F-FDG PET/CT in NSCLC, 40P had excellent inter-operator reproducibility of texture features and has proven tolerable in previous studies[18]. It is also recommended for heterogeneity determination of lesions affected by respiratory migration[19].

VOI was set not to include physiological accumulation. We calculated The SUV parameters of SUV$_{max}$, SUV$_{peak}$, SUV$_{mean}$, MTV, TLG as well as fifty-six texture parameters derived from seven matrices for each VOI. SUV$_{peak}$ is defined as the mean SUV in an 1 cm^3 sphere around the pixel with the highest uptake and is assumed to be less affected by image noise than SUV$_{max}$. For images with noise properties typically associated with clinical PET images, SUV$_{peak}$ can provide a slightly more robust alternative. To extract the texture parameters, we first equalized histograms by rescaling the intensity within each ROI between the 1st and 99th percentiles of the ROI over 64 bins. Using 64 equally divided bins has been a common approach for image quantitation in radiomics analysis, and it also allows exploration of entire ranges of tumor signal intensity[20].

Statistical analysis.   We compared all data between NSCLC and RP after CIRT using Wilcoxon rank-sum tests. Values lying nearest the upper left corner in ROC curves were considered to indicate optimal diagnostic accuracy. Sensitivity, specificity, and accuracy were calculated using appropriate cutoffs. Diagnostic accuracy was compared using areas under ROC curves (AUC), and ROC curves were also compared. All data were statistically analyzed using JMP v.14.2.0 software (SAS Institute Inc., Cary, NC, USA) and values with P < 0.05 were considered statistically significant.

Characteristics	NSCLC (n = 32)	RP (n = 31)	p value
Mean age (y)	76.8 ± 8.2	79.2 ± 7.7	0.322
Gender			
Male	24	23	
Female	8	8	
Histology			
Squamous cell carcinoma	6	4	
Adenocarcinoma	18	15	
Neuroendocrine carcinoma	1	1	
Unclassified non-small cell carcinoma	7	11	
Tumor size (cm)	2.90 ± 1.59	5.08 ± 2.12	< 0.0001*

Table 1. Characteristic of patients with NSCLC and RP. *P < 0.05, statistically significant. NSCLC, non-small cell lung carcinoma; RP, radiation pneumonitis; SCC, squamous cell carcinoma.

Results

Characteristics of patients with NSCLC and RP. The 63 patients (age, 76.8 ± 8.2 years; male, n = 47 [74.6%]) included eight with squamous cell carcinoma (SCC), 33 with adenocarcinoma (ADC), 2 with neuroendocrine carcinoma, and 18 with unclassified non-small cell carcinoma. The sizes of the NSCLC and RP were 2.90 ± 1.59 (range, 71.9–19.0) and 5.08 ± 2.12 (range, 82.4–33.4) cm, respectively. Gender, and tumor size significantly differed between the NSCLC and RP groups (P < 0.05; Table 1).

Comparison of NSCLC and RP. Statistical differences among parameters in the texture analysis were explored using Wilcoxon rank-sum tests (Table 2). Most texture parameters significantly differed between NSCLC and RP (P < 0.05), whereas most SUV parameters did not.

Diagnostic accuracy. Figures 1 and 2 show the outcomes of ROC analyses for each parameter. The AUC of SUV_{max}, SUV_{peak}, MTV and TLG were respectively, 0.64, 0.63, 0.86 and 0.75. On the other hand, the AUC of the gray-level run-length matrix run percentage (GLRLM) and neighborhood gray-tone difference matrix coarseness (NGTDM) were 0.83 and 0.82, respectively, and significantly differed from the AUC of the SUV_{max} (Table 3).

Comparison of NSCLC and RP images. Figure 3 shows representative images. The GLRLM run percentage and NGTDM coarseness were significantly higher in NSCLC, than in RP, whereas SUV_{max} values of both lesions were similar.

Discussion

To develop the differential diagnosis of malignancy and benign lesions, we compared whether texture parameters could more accurately differentiate NSCLC from RP in patients after CIRT than SUV parameters such as SUV_{max} and MTV. We found a possible relationship of textural imaging parameters for GLRLM run percentage and NGTDM coarseness of tumor heterogeneity measured on ^{18}F-FDG PET/CT images, which would lead the ability to differentiate RP from NSCLC.

The MTV and TLG were significantly increased, whereas the SUV_{max} was reduced in RP compared with NSCLC. Buyger et al. reported that a fixed threshold could substantially underestimate TLG and MTV in lesions with high ^{18}F-FDG uptake[21]. Therefore, a decrease in SUV_{max} might erroneously increase MTV because a larger volume of a less active tumor will be included in the MTV[22]. The SUV is not helpful for differentiating benign from malignant lesions[23], and MTV and TLG are calculated based on SUV. Thus, we considered that MTV and TLG are not suitable for differentiating NSCLC and RP.

Almost all texture parameters significantly differed and had significantly better diagnostic ability than SUV_{max}. In particular, the GLRLM run percentage and NGTDM coarseness would be appropriate parameters due to their high diagnostic accuracy. The GLRLM run percentage corresponded to the number of homogeneous runs of a specific intensity voxel within an image. We found that the GLRLM run percentage was significantly reduced in RP compared with NSCLC. This suggests that ^{18}F-FDG accumulation is more heterogeneous in NSCLC than in RP. Hotta et al. reported that the GLRLM run percentage using a machine learning in[11]C-methionine PET images could distinguish recurrent brain tumors from radiation necrosis and that radiation necrosis was significantly reduced compared with recurrent brain tumors[24]. Adding the machine learning model might allow to create a model with higher sensitivity and specificity than this model proposed for benign and malignant lung differentiation. The NGTDM coarseness is based on differences between each voxel and neighboring voxels in adjacent image planes, and thus measures granularity within an image[25]. Chen et al. found significantly lower NGTDM coarseness in benign than malignant solitary pulmonary nodules[26]. The present findings revealed significantly lower NGTDM coarseness in RP than NSCLC, which is considered to reflect biological differences between benign and malignant lesions. Also, NGTDM coarseness is useful in discriminating benign and malignant cancers of the head and neck[27].

The present findings of texture features are considered to reflect the heterogeneity of ^{18}F-FDG accumulation in lesions. Several studies have found that the intratumoral heterogeneity of ^{18}F-FDG uptake in tumors might

Parameter	NSCLC (n = 32)	RP (n = 31)	p value
SUV$_{max}$	4.95 ± 4.89	1.86 ± 0.71	0.063
SUV$_{peak}$	4.31 ± 4.43	1.67 ± 0.62	0.084
SUV$_{mean}$	2.96 ± 2.99	1.09 ± 0.41	0.080
MTV	8.64 ± 6.87	40.20 ± 25.84	< 0.0001*
TLG	31.11 ± 50.38	47.10 ± 35.27	0.001*
GLRLM			
Short Runs Emphasis mean	0.85 ± 0.32	0.92 ± 0.17	< 0.0001*
Short Runs Emphasis max	0.86 ± 0.32	0.94 ± 0.17	< 0.0001*
Long Runs Emphasis mean	0.98 ± 0.38	1.19 ± 0.22	< 0.0001*
Long Runs Emphasis max	1.04 ± 0.40	1.30 ± 0.26	< 0.0001*
Gray Level Nonuniformity mean	2.15 ± 2.38	7.78 ± 10.00	0.001*
Gray Level Nonuniformity max	2.30 ± 2.63	8.16 ± 10.46	0.006*
Run Length Nonuniformity mean	4.08 ± 4.09	14.83 ± 17.54	0.004*
Run Length Nonuniformity max	4.48 ± 4.69	16.08 ± 18.93	0.003*
Run Percentage mean	0.81 ± 0.31	0.84 ± 0.16	< 0.0001*
Run Percentage max	0.83 ± 0.32	0.88 ± 0.16	< 0.0001*
GLSZM			
High Intensity Emphasis	495.05 ± 224.06	473.08 ± 181.11	0.085
Low Intensity Emphasis	0.05 ± 0.02	0.04 ± 0.02	0.001*
Large Area Emphasis	1.20 ± 0.50	1.70 ± 0.38	< 0.0001*
Small Area Emphasis	0.68 ± 0.27	0.62 ± 0.13	< 0.0001*
Intensity Variability	1.43 ± 1.09	4.17 ± 4.54	0.012*
Run Length Variability	2.17 ± 1.41	5.64 ± 5.17	0.008*
Zone Percentage	0.65 ± 0.26	0.56 ± 0.12	< 0.0001*
NGLCM3D			
Uniformity mean	0.00 ± 0.00	0.00 ± 0.00	0.010*
Uniformity max	0.00 ± 0.00	0.00 ± 0.00	0.188
Entropy mean	5.44 ± 2.10	6.52 ± 1.21	0.001*
Entropy max	5.51 ± 2.13	6.70 ± 1.25	< 0.0001*
Dissimilarity mean	7.78 ± 3.55	5.42 ± 1.32	< 0.0001*
Dissimilarity max	9.96 ± 4.48	7.09 ± 2.00	< 0.0001*
Contrast mean	110.91 ± 64.96	50.31 ± 17.80	< 0.0001*
Contrast max	172.44 ± 97.36	81.64 ± 35.67	< 0.0001*
Homogeneity mean	0.17 ± 0.08	0.25 ± 0.05	< 0.0001*
Homogeneity max	0.23 ± 0.10	0.34 ± 0.07	< 0.0001*
Correlation mean	0.03 ± 0.02	0.01 ± 0.01	< 0.0001*
Correlation max	0.03 ± 0.03	0.01 ± 0.01	< 0.0001*
NGLCM3DMean			
Uniformity	0.00 ± 0.00	0.00 ± 0.00	0.318
Entropy	5.24 ± 2.01	6.05 ± 1.14	0.028*
Dissimilarity	4.27 ± 1.98	3.18 ± 0.88	< 0.0001*
Contrast	33.18 ± 20.16	20.06 ± 10.79	0.003*
Homogeneity	0.25 ± 0.11	0.36 ± 0.08	< 0.0001*
Correlation	0.04 ± 0.03	0.01 ± 0.01	< 0.0001*
NGLCM			
Uniformity mean	0.00 ± 0.00	0.00 ± 0.00	0.036*
Uniformity max	0.00 ± 0.00	0.00 ± 0.00	0.199
Entropy mean	5.42 ± 2.09	6.42 ± 1.20	0.001*
Entropy max	5.49 ± 2.11	6.59 ± 1.23	0.0003*
Dissimilarity mean	6.84 ± 3.12	4.60 ± 1.16	< 0.0001*
Dissimilarity max	8.43 ± 3.78	5.80 ± 1.54	< 0.0001*
Contrast mean	84.82 ± 49.77	35.32 ± 13.09	< 0.0001*
Contrast max	122.78 ± 69.72	53.65 ± 21.36	< 0.0001*
Homogeneity mean	0.18 ± 0.08	0.28 ± 0.06	< 0.0001*
Homogeneity max	0.22 ± 0.10	0.33 ± 0.07	< 0.0001*
Inverse Difference Moment mean	0.11 ± 0.06	0.19 ± 0.05	< 0.0001*
Continued			

Parameter	NSCLC (n = 32)	RP (n = 31)	p value
Inverse Difference Moment max	0.14 ± 0.07	0.24 ± 0.07	< 0.0001*
Correlation mean	0.03 ± 0.03	0.01 ± 0.01	< 0.0001*
Correlation max	0.03 ± 0.03	0.01 ± 0.01	< 0.0001*
NGTDM			
Coarseness	0.01 ± 0.00	0.00 ± 0.00	< 0.0001*
Contrast	0.00 ± 0.00	0.00 ± 0.00	< 0.0001*
Busyness	0.18 ± 0.14	0.80 ± 0.52	< 0.0001*
Complexity	45.72 ± 43.20	7.40 ± 4.85	< 0.0001*
Strength	6.30 ± 4.23	2.29 ± 1.89	< 0.0001*
SUV Histogram			
Variance	208.68 ± 88.57	195.13 ± 52.23	0.001*
Entropy	3.38 ± 1.29	3.73 ± 0.70	0.922

Table 2. Significant difference of each parameters. *P < 0.05, statistically significant.
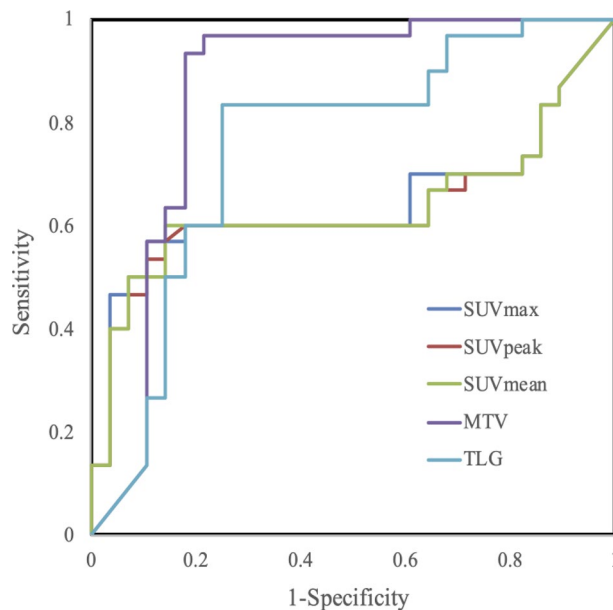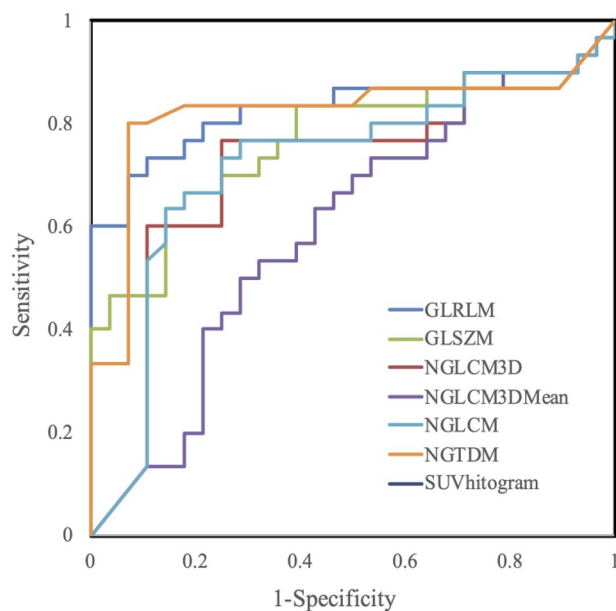

Figure 1. Receiver operating characteristic curves of ability of SUV parameters to discriminate NSCLC from RP.

be useful for evaluating therapeutic responses and predicting prognoses of NSCLC[20,28,29], while there is a review paper by Han, S. et al., showing limited evidence to support the prognostic value of texture analysis in ^{18}F-FDG PET in lung cancer[30]. Yet, little is understood about the application of ^{18}F-FDG PET/CT texture analysis to the differential diagnosis of NSCLC and RP. The effects of CIRT on NSCLC can be highly beneficial. The application of ^{18}F-FDG PET/CT texture analysis should improve the ability to distinguish NSCLC from RP. If so, then the amount of time required to determine a treatment regimen such as repeated irradiation could be decreased.

Most ^{18}F-FDG PET/CT texture parameters (51 out of 56 parameters; Table 2) were useful for differentiating NSCLC from RP after CIRT. Gunma University has recently reported that SUV_{max} and MTV had better predictive or prognostic power for CIRT-treated NSCLC patients[31,32]. Metabolic information of ^{18}F-FDG PET/CT imaging reflects a biological property of tumor as well as metabolically diverse components, including inflammatory tissues and surrounding normal tissues such as vessels, bronchi, and pleura after CIRT[29,33]. ^{18}F-FDG PET/CT is considered to be playing key metabolic imaging in the management of CIRT for NSCLC.

This study had some limitations. Texture parameters could be affected by lesion size, histological tumor type, and inflammatory status[31]. The textural analysis also requires evaluation of so many variables, and the sample size is relatively small for this number of variables. Therefore, further studies in more patients with different types of tumors are needed. In addition, due to the limited spatial resolution of PET, image noise and partial volume effects may affect the results of this study[33].

Figure 2. Receiver operating characteristic curves of ability of texture parameters to discriminate NSCLC from RP. GLRLM, gray-level run-length matrix run percentage; GLSZM, gray-level size-zone matrix intensity variability; NGLCM, normalized gray-level cooccurrence matrix dissimilarity; NGTDM, neighborhood gray-tone difference matrix coarseness; SUV Histogram, SUV histogram variance.

Parameter	Cutoff	Sensitivity (%)	Specificity (%)	PPV (%)	NPV (%)	AUC
SUV_{max}	2.80	56.67	10.71	85.00	65.79	0.64
SUV_{peak}	2.64	53.33	10.71	84.21	64.10	0.63
SUV_{mean}	1.54	60.00	14.29	81.82	66.67	0.63
MTV	16.37	93.33	17.86	84.85	92.00	0.86
TLG	27.88	83.33	25.00	78.13	80.77	0.75
GLRLM	0.43	70.00	7.14	91.30	74.29	0.83
GLSZM	0.16	60.00	14.29	81.82	66.67	0.76
NGLCM3D	0.17	76.67	25.00	76.67	75.00	0.71
NGLCM3DMean	0.24	50.00	28.57	65.22	57.14	0.59
NGLCM	0.15	63.33	14.29	82.61	68.57	0.72
NGTDM	0.00	80.00	7.14	92.31	81.25	0.82
SUV Histogram	0.92	40.00	3.57	92.31	60.00	0.65

Table 3. ^{18}F-FDG PET/CT metrics and cutoffs for differentiation between NSCLC and RP. *P < 0.05, statistically significant. AUC, area under ROC curve; GLRLM, gray-level run-length matrix run percentage; GLSZM, gray-level size-zone matrix intensity variability; NSCLC, non-small cell lung carcinoma; NGLCM, normalized gray-level cooccurrence matrix dissimilarity; NGTDM, neighborhood gray-tone difference matrix coarseness; NPV, negative predictive value; PPV, positive predictive value; RP, radiation pneumonitis; SUV Histogram, SUV histogram variance.

Conclusion

We determined that texture parameters can differentiate NSCLC from RP after CIRT more accurately than SUV parameters such as SUV_{max} and MTV. The intratumoral heterogeneity of ^{18}F-FDG uptake evaluated by texture analysis yielded improved diagnostic ability for differentiating NSCLC from RP after CIRT that outperformed
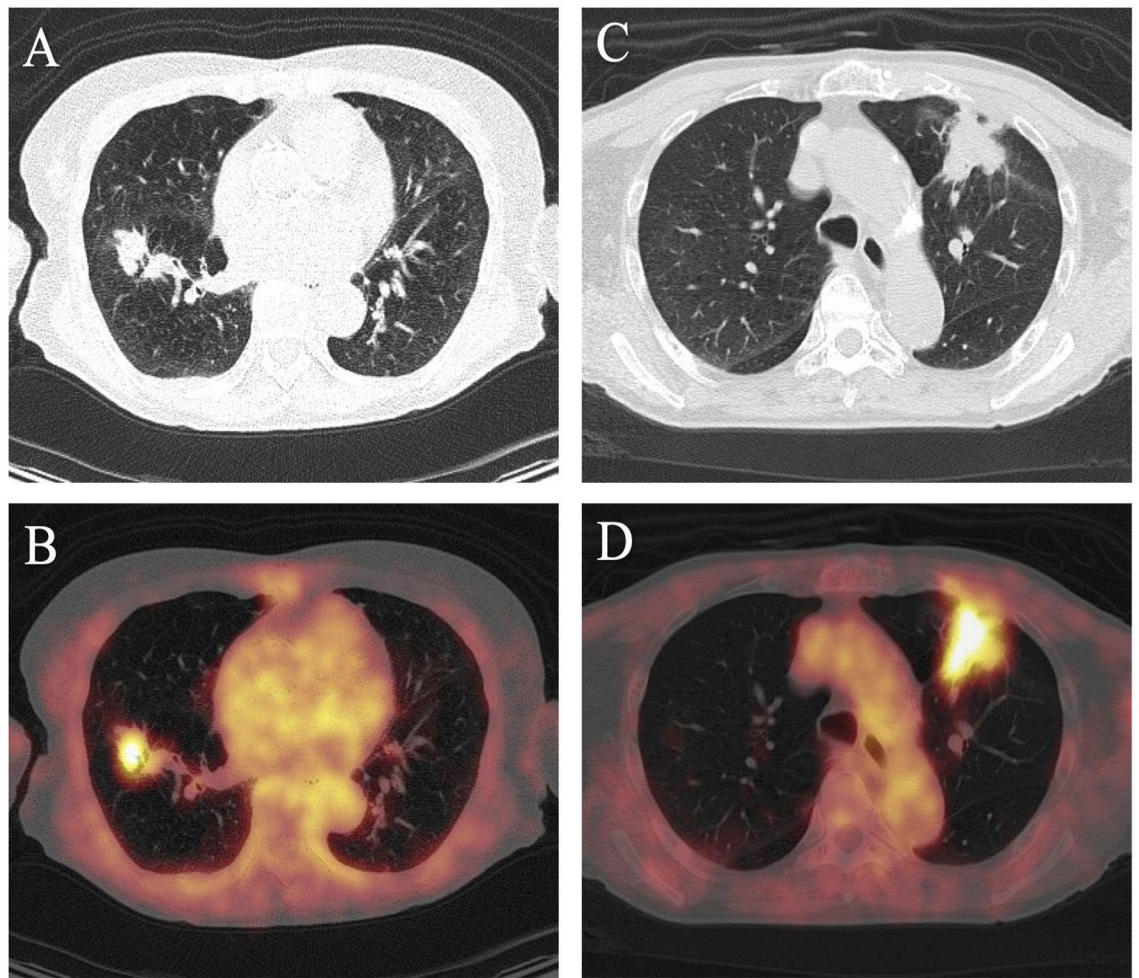
Figure 3. Representative CT and fused PET/CT images of NSCLC and RP. (**A**) CT image shows mass in right middle lobe of 79-year-old male with NSCLC. (**B**) Axial fused PET/CT image shows high ^{18}F-FDG uptake (SUV$_{max}$, 4.32) and heterogeneous ^{18}F-FDG distribution (GLRLM run percentage, 0.81; NGTDM coarseness, 0.0068). (**C**) CT Image of 77-year-old male with RP shows mass-like attenuation in left upper lobe. (**D**) Axial fused PET/CT image shows high ^{18}F-FDG uptake (SUV$_{max}$, 3.75) and homogeneous ^{18}F-FDG distribution (GLRLM run percentage, 0.65; GLSZM coarseness, 0.0017).

SUV. In particular, GLRLM run percentage and NGTDM coarseness are appropriate parameters with high diagnostic accuracy. Our findings provide important information for understanding ^{18}F-FDG PET/CT imaging in the management of CIRT for NSCLC.

References

1. Novello, S. *et al.* Metastatic non-small-cell lung cancer: ESMO Clinical Practice Guidelines for diagnosis, treatment and follow-up. *Ann Oncol.* **27**, v1–v27 (2016).
2. Chua, K. L. M., Sin, I., Fong, K. W., Chua, M. L. K. & Onishi, H. Stereotactic body radiotherapy for early stage lung cancer-historical developments and future strategies. *Chin Clin Oncol.* **6**, S20 (2017).
3. Liao, Z. & Simone, C. B. 2nd Particle therapy in non-small cell lung cancer. *Transl Lung Cancer Res.* **7**, 141–152 (2018).
4. Kanai, T. *et al.* Biophysical characteristics of HIMAC clinical irradiation system for heavy-ion radiation therapy. *Int. J. Radiat. Oncol. Biol. Phys.* **44**, 201–210 (1999).
5. Abdollahi, A. *et al.* Inhibition of platelet-derived growth factor signaling attenuates pulmonary fibrosis. *J. Exp. Med.* **201**, 925–935 (2005).
6. Graves, P. R., Siddiqui, F., Anscher, M. S. & Movsas, B. Radiation pulmonary toxicity: from mechanisms to management. *Semin. Radiat. Oncol.* **20**, 201–207 (2010).
7. Nishimura, H. *et al.* Radiographic pulmonary and pleural changes after carbon ion irradiation. *Int. J. Radiat. Oncol. Biol. Phys.* **55**, 861–866 (2003).
8. Hayashi, K. *et al.* Prognostic analysis of radiation pneumonitis: carbon-ion radiotherapy in patients with locally advanced lung cancer. *Radiat. Oncol.* **12**, 91 (2017).
9. Bury, T. *et al.* Value of FDG-PET in detecting residual or recurrent nonsmall cell lung cancer. *Eur. Respir. J.* **14**, 1376–1380 (1999).

10. Wong, R. J. *et al.* Diagnostic and prognostic value of [¹⁸F]fluorodeoxyglucose positron emission tomography for recurrent head and neck squamous cell carcinoma. *J. Clin. Oncol.* **20**, 4199–4208 (2002).
11. Hellwig, D. *et al.* Diagnostic performance and prognostic impact of FDG-PET in suspected recurrence of surgically treated non-small cell lung cancer. *Eur. J. Nucl. Med. Mol. Imaging.* **33**, 13–21 (2006).
12. Juweid, M. E. & Cheson, B. D. Positron-emission tomography and assessment of cancer therapy. *N. Engl. J. Med.* **354**, 496–507 (2006).
13. Park, G. C. *et al.* Prognostic value of metabolic tumor volume measured by 18F-FDG PET/CT in advanced-stage squamous cell carcinoma of the larynx and hypopharynx. *Ann. Oncol.* **24**, 208–214 (2013).
14. Chen, W. *et al.* Quantitative assessment of metabolic tumor burden in molecular subtypes of primary breast cancer with FDG PET/CT. *Diagn. Interv. Radiol.* **24**, 336–341 (2018).
15. Amadasun, M. & King, R. Textural features corresponding to textural properties. *IEEE Trans. Syst. Man Cybern.* **19**, 1264–1274 (1989).
16. Yu, H. *et al.* Automated radiation targeting in head-and-neck cancer using region-based texture analysis of PET and CT images. *Int. J. Radiat. Oncol. Biol. Phys.* **75**, 618–625 (2009).
17. Sugihara, T. *et al.* Bone metastases from breast cancer: associations between morphologic CT patterns and glycolytic activity on PET and bone scintigraphy as well as explorative search for influential factors. *Ann. Nucl. Med.* **31**, 719–725 (2017).
18. Bashir, U. *et al.* The effects of segmentation algorithms on the measurement of (18)F-FDG PET texture parameters in non-small cell lung cancer. *EJNMMI Res.* **7**, 60 (2017).
19. Carles, M. *et al.* Evaluation of PET texture features with heterogeneous phantoms: complementarity and effect of motion and segmentation method. *Phys. Med. Biol.* **62**, 652–668 (2017).
20. Giannini, V. *et al.* Predicting locally advanced rectal cancer response to neoadjuvant therapy with (18)F-FDG PET and MRI radiomics features. *Eur. J. Nucl. Med. Mol. Imaging.* **46**, 878–888 (2019).
21. Burger, I. A. *et al.* PET quantification with a histogram derived total activity metric: superior quantitative consistency compared to total lesion glycolysis with absolute or relative SUV thresholds in phantoms and lung cancer patients. *Nucl. Med. Biol.* **41**, 410–418 (2014).
22. Burger, I. A. *et al.* 18F-FDG PET/CT of non-small cell lung carcinoma under neoadjuvant chemotherapy: background-based adaptive-volume metrics outperform TLG and MTV in predicting histopathologic response. *J. Nucl. Med.* **57**, 849–854 (2016).
23. Shim, S. S. *et al.* Focal parenchymal lung lesions showing a potential of false-positive and false-negative interpretations on integrated PET/CT. *AJR Am J Roentgenol.* **186**, 639–648 (2006).
24. Hotta, M., Minamimoto, R. & Miwa, K. 11C-methionine-PET for differentiating recurrent brain tumor from radiation necrosis: radiomics approach with random forest classifier. *Sci. Rep.* **9**, 15666 (2019).
25. Cook, G. *et al.* Radiomics in PET: Principles and applications. *Clin. Transl. Imaging.* **2**, 269–276 (2014).
26. Chen, S. *et al.* Using neighborhood gray tone difference matrix texture features on dual time point PET/CT images to differentiate malignant from benign FDG-avid solitary pulmonary nodules. *Cancer Imaging* **19**, 56 (2019).
27. Yu, H., Caldwell, C., Mah, K. & Mozeg, D. Coregistered FDG PET/CT-based textural characterization of head and neck cancer for radiation treatment planning. *IEEE Trans. Med. Imaging.* **28**, 374–383 (2009).
28. Nakajo, M. *et al.* A pilot study of texture analysis of primary tumor [(18)F]FDG uptake to predict recurrence in surgically treated patients with non-small cell lung cancer. *Mol Imaging Biol.* **21**, 771–780 (2019).
29. Bashir, U., Siddique, M. M., McLean, E., Goh, V. & Cook, G. J. Imaging heterogeneity in lung cancer: techniques, applications, and challenges. *AJR Am. J. Roentgenol.* **207**, 534–543 (2016).
30. Han, S. *et al.* A systematic review of the prognostic value of texture analysis in 18F-FDG PET in lung cancer. *Ann. Nucl. Med.* **32**, 602–610 (2018).
31. Shirai, K. *et al.* Maximum standardized uptake value on FDG-PET predicts survival in stage I non-small cell lung cancer following carbon ion radiotherapy. *Oncol. Lett.* **13**, 4420–4426 (2017).
32. Shrestha, S. *et al.* Prognostic significance of semi-quantitative FDG-PET parameters in stage I non-small cell lung cancer treated with carbon-ion radiotherapy. *Eur. J. Nucl. Med. Mol. Imaging.* **47**, 1220–1227 (2020).
33. Miwa, K. *et al.* FDG uptake heterogeneity evaluated by fractal analysis improves the differential diagnosis of pulmonary nodules. *Eur. J. Radiol.* **83**, 715–719 (2014).

Acknowledgements

Author contributions

R.N. and M.S. were responsible for the research, wrote the main manuscript text as the first author (M.S.) and the corresponding author (R.N.) responsible for this study, and coordinated and supervised the entire study. K.M., Y.K., and K.T. is a radiological technologist who were responsible for PET/CT scan and provided technical advice for PET/CT imaging. N.Y. and H.T. are radiation oncologists responsible for planning patient examinations, therapy, and subsequent management of patients. RK and MK engaged the imaging data analysis and statistical analysis for the texture analysis. K.Y., K.T., and T.H., interpreted PET/CT images. All authors conducted this study and also read and approved the final version of the manuscript.

Competing interests

The authors declare no competing interests.

Additional information

Correspondence and requests for materials should be addressed to R.N.

Reprints and permissions information is available at www.nature.com/reprints.

Publisher's note Springer Nature remains neutral with regard to jurisdictional claims in published maps and institutional affiliations.